C-Statistic vs Bayesian: A Comparative Analysis of X-ray Spectral Statistics

by

David Koranteng

A THESIS SUBMITTED IN PARTIAL FULFILMENT OF
THE REQUIREMENTS FOR THE DEGREE OF

BACHELOR OF SCIENCE

in

Honours Astrophysics

(Department of Astronomy and Physics, Dr. Luigi C. Gallo supervising faculty)

....

....

....

....

....

SAINT MARY'S UNIVERSITY

April 17, 2023

© David Koranteng, 2023

Abstract

C-Statistic vs Bayesian: A Comparative Analysis of X-ray Spectral
Statistics

by *David Koranteng*

submitted on April 17, 2023:

The X-ray spectra of active galactic nuclei (AGN) contain many spectral features, such as emission lines, that provide much insight into the inner workings of these objects. In a class of AGN known as Narrow-Line Seyfert 1 (NLS1) galaxies, analyzing these spectral features can provide especially useful insight into the internal structure due to their orientation. Using two different statistical methods (Bayesian X-ray Analysis and C-Statistic) to analyze the spectra of 21 NLS1 galaxies, it can be determined which method is superior at detecting emission lines in the spectra. It is found that C-Statistic may be superior at detecting lines in low-count spectra, but BXA has separate advantages that may lead to more success at detecting lines in real sources.

Contents

List of Figures

Chapter 1

INTRODUCTION

1.1 ACTIVE GALAXIES

At the centre of all major galaxies lies a black hole, called a **supermassive black hole**, or *SMBH*, which has a mass that can be millions to billions of times the mass of the Sun. In galaxies such as our own, the central black hole is relatively dormant. It can be observed in several wavelengths due to the process of the black hole accreting surrounding in-falling material, but this accretion process is tame compared to other central SMBHs. There is a classification of galaxies known as **Active Galaxies** that are designated as such due to their central black holes being comparatively much more active (Peterson, 2009).

The accretion process in the centre of these active galaxies is significantly more violent, resulting in the emission of electromagnetic radiation across the entire EM spectrum, often outshining stellar emission from the entire rest of the galaxy. Since these highly energetic central engines are the main source of emission in these galaxies, they are called **Active Galactic Nuclei**, or *AGN*.

1.1.1 INTERNAL STRUCTURE

AGN have been observed in every band of the electromagnetic spectrum due to several internal processes producing various types of EM emission. Therefore, by observing and analyzing spectra in specific bands of light, a general description of the internal structure of AGN can be determined.

AGN observation is particularly useful in X-ray due to the strength of the emission in this band. As previously stated, AGN often outshine the stellar emission from elsewhere in the galaxy. This is particularly notable when these active galaxies are observed in X-ray. X-ray images of AGN often highlight a very bright central region that is more difficult to discern from stellar light when viewed in optical. X-ray spectra of AGN contain several features that provide insight into the structure of AGN. In the 0.3-10 keV energy band of X-rays, the notable features include certain emission lines and absorption edges. Additionally, the shape of the continuum in these spectra also contains valuable information.

This continuum has three discernible trends. Beginning at 0.3 keV, there is a bump in energy that starts to flatten around 2 keV and then steadily decreases in the shape of a power law. This power law trend continues as the main continuum until another bump in energy begins around 10 keV and continues to higher energies. This initial bump from approximately 0.3-2 keV is known as the *soft excess*. The bump in higher energies beginning around 10 keV is known as the *Compton Hump*. The flat, power law-like portion of the continuum is important, as the slope of this part can help attribute the emission to specific processes. The observed continuum is

the result of two overlapping spectra: a primary emission spectrum and a reflection spectrum (See Figure 1.1).

The primary spectrum is produced by a cloud of plasma surrounding the accretion disk, known as the *corona*. The process of accretion creates emission in the UV portion of the EM spectrum. This UV light is emitted away from the disk into the surrounding corona, where it gains energy through a process called *inverse Compton scattering*, or *Comptonization*. The UV photons collide with the electrons in the corona and take energy from them in the collision. As a result of this process happening continuously
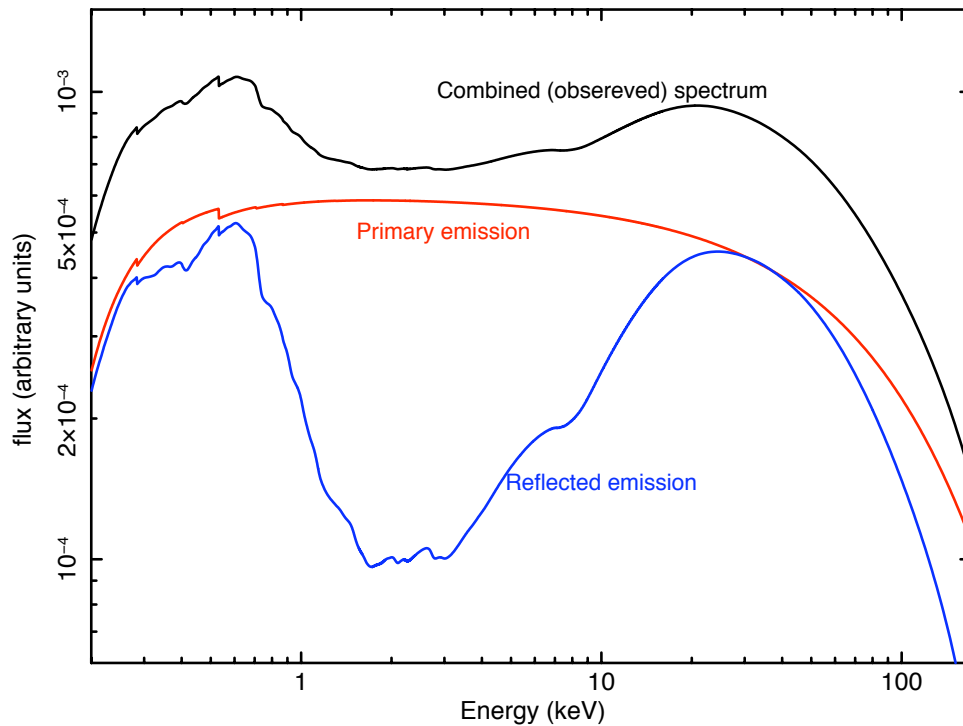
Figure 1.1: An example of the continuum spectrum of an AGN viewed in the X-ray band, represented as a combined spectrum (black) of two separate spectra, a primary (red) spectrum and a reflected (blue) spectrum (Gallo, 2011).

in the corona, the photons enter from the accretion disk as UV light and are up-scattered to the X-rays that are observed as the primary spectrum. However, these X-rays are re-emitted by the corona isotropically, and therefore some are emitted away from the observer. These X-ray photons are emitted towards the accretion disk, and are then reflected towards to observer as an altered reflection spectrum (See Figure 1.2). These two spectra combine when observed, and the result is the continuum previously described.

The most notable feature present in the X-ray spectrum of an AGN is a spike in the continuum around 6.4-7 keV, which matches a set of iron emission lines: Fe-Kα_1, Fe-Kα_2, and Fe-Kβ. These emission lines indicate the presence of iron within the system, and by analyzing the broadening of the emission line(s), the proximity of the iron to the central black hole can be determined.

These conclusions can be drawn due to relativistic effects on the line profile that would become apparent if the iron was in close proximity to the black hole. Knowing
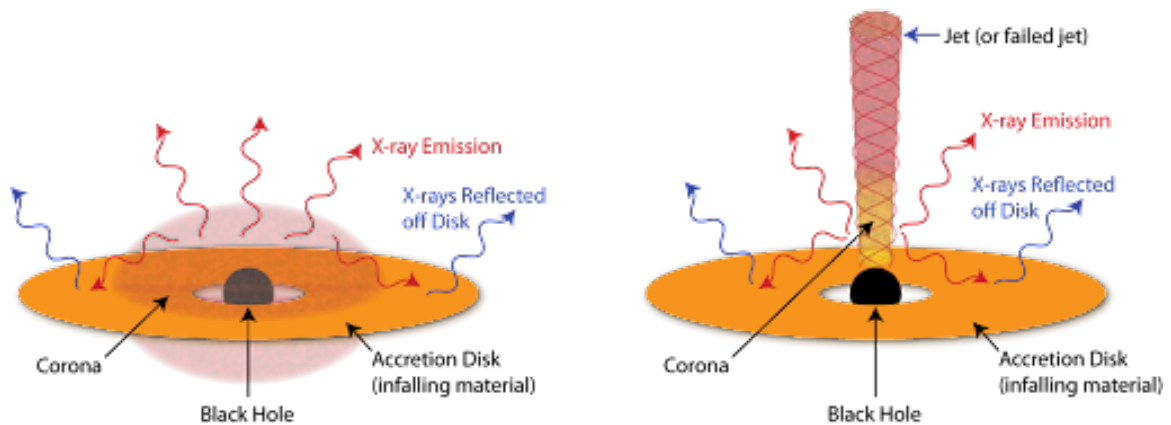
Figure 1.2: X-rays produced in the corona are emitted in all directions. Emission sent away from the observer and towards the accretion disk is then reflected back in the direction of the observer. Left figure depicts a standard corona model. Right image depicts a jet (See Figure 1.4) whose base acts as a corona (Wilkins, 2017).

what an intrinsic Fe-Kα emission line looks like, it can then be compared to the emission line present in the spectrum, and the differences can be attributed to physical processes. Firstly, if the emitting iron is present in the accretion disk, it is expected that the motion in the accretion disk would lead to the emission line undergoing Doppler broadening. If the iron is closer to the black hole, its profile will be further broadened due to special relativistic effects, such as beaming. (See Figure 1.3). Lastly, if the iron is in extremely close proximity to the black hole, it will be subject to extreme broadening, with a strong shift to low energy. This is due to *gravitational redshift*, an effect where photons lose energy when escaping a gravitational well (Gallo, 2011).

AGN are also powerful radio sources, particularly due to synchrotron emission (Peterson, 2009). Synchrotron emission is the emission produced by relativistic charged particles being accelerated in a magnetic field and moving in a helical path. This emission is beamed in the direction of motion of the charged particles. This radio emission can often be observed in the shape of large collimated structures emerging from the central engine of the active galaxy. (See Figure 1.4)

This type of radio emission is not always observed in AGN, however. When AGN are observed to have excess radio emission compared to other bands, such as optical, they are considered *radio loud*. Otherwise, they are designated as *radio quiet* if their radio emission is not proportionately more luminous than their optical emission.

In order to account for observed differences in AGN spectra, the physical nature of AGN is described using a single simple model (Sparke, 2007). The model, called *unification theory*, describes AGN as one type of object that is viewed from different

orientations, and these orientations cause spectral and observation differences.
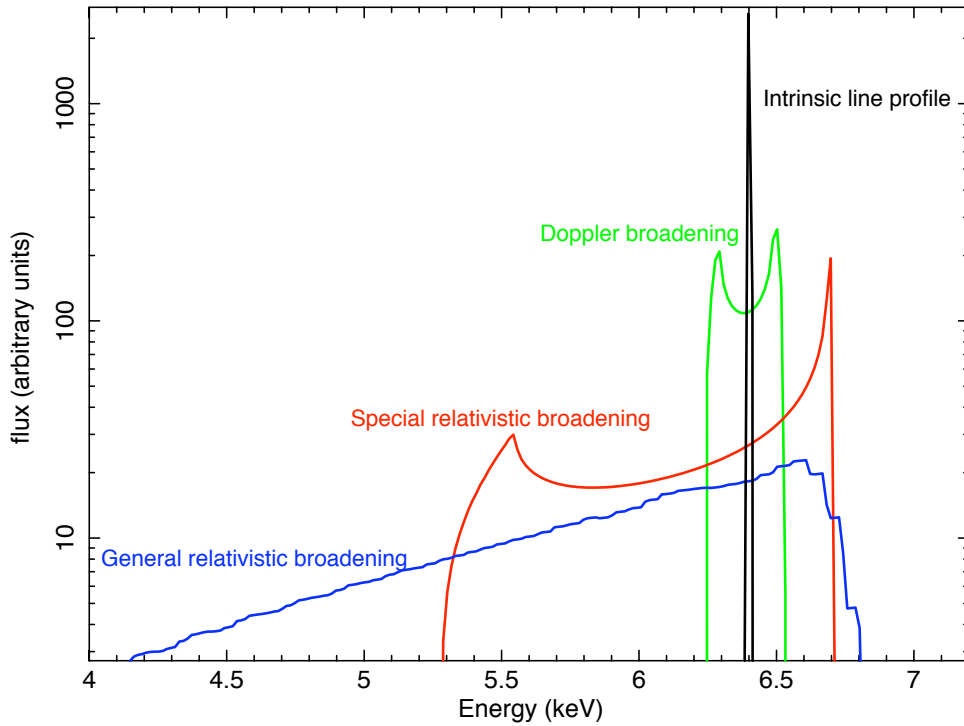
Figure 1.3: The original emission line is emitted at 6.4 keV (black). The line profile gains a two-prong shape when subject to the Doppler effect (green). In closer proximity to the black hole, the line broadens due to special relativistic effects, resulting in the line profile becoming asymmetric (red). Lastly, the original line becomes extremely asymmetrically broadened due to general relativity (blue) (Gallo, 2011).

1.1.2 NARROW-LINE SEYFERT 1 GALAXIES

Narrow-Line Seyfert 1 (*NLS1*) galaxies are a type of galaxy within the AGN subclass known as Seyfert galaxies. Seyfert galaxies are active galaxies classified by the X-ray luminosity of the nucleus. They have nuclei with luminosity values within the range of 2 x $10^8 L_\odot$ - 10^{11} $L_\odot$. They also have optical spectra containing

prominent emission lines, (Sparke, 2007). Seyferts are divided into two types based on the profiles of these emission lines. Seyfert 1 galaxies display an assortment of optical emission lines in their spectra that can be grouped into both narrow and broad portions; Seyfert 2 galaxies, alternatively, only display narrow lines (Peterson, 2009).

As can be seen in Figure 1.5, Seyfert 1 galaxies display both narrow and broad lines because they are observed from an orientation in which the broad-line region is unobstructed. This means that Seyfert 1s provide an optimal viewing angle when studying the internal accretion disk system of AGNs.

Narrow-Line Seyfert 1s are their own subclass of Seyfert 1s. This designation of
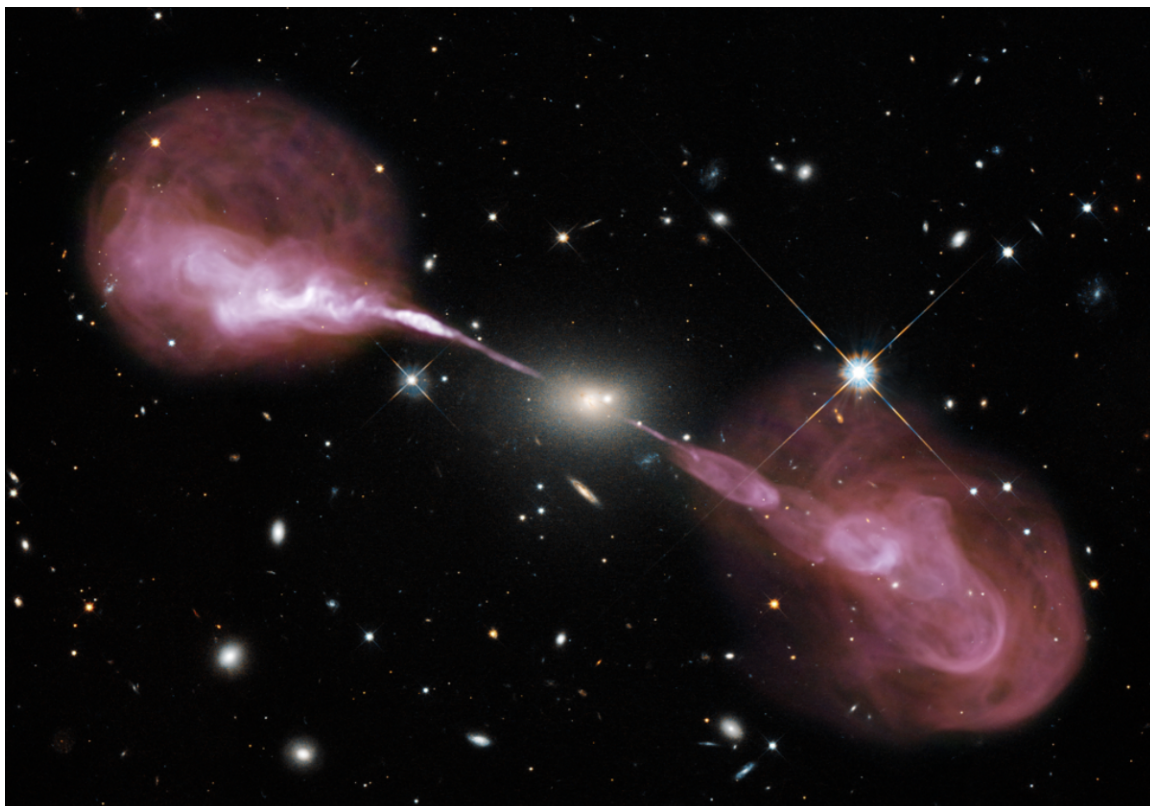
Figure 1.4: An optical image of galaxy Hercules A with a radio image overlayed in pink. In radio band, large elongated jets become visible (NASA et al., 2012).
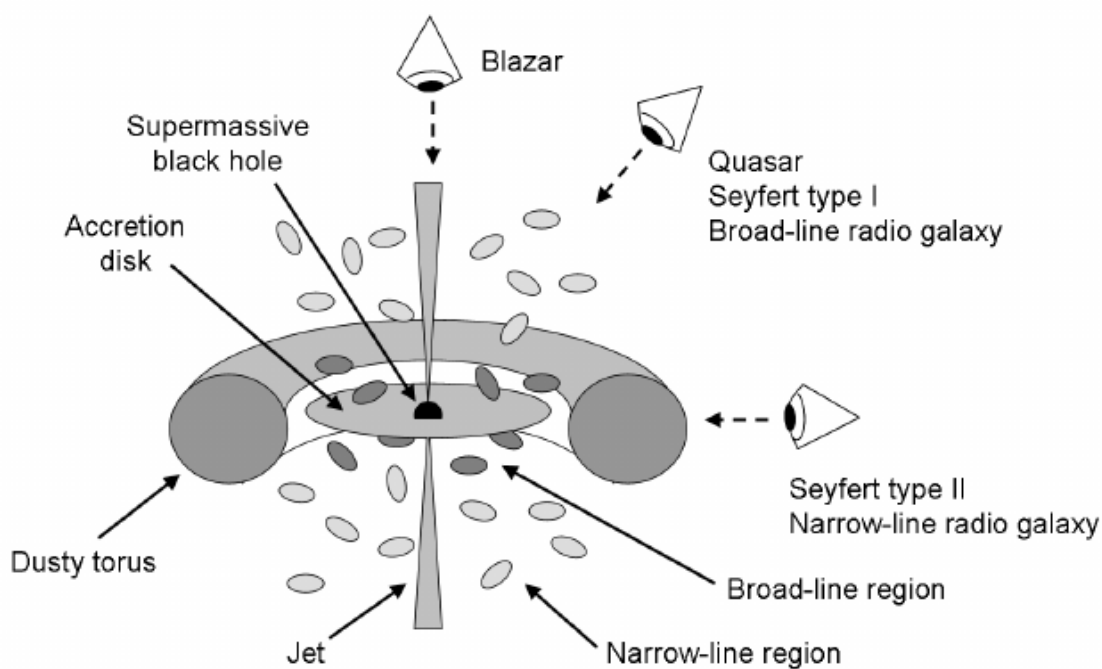
Figure 1.5: Unification Theory proposes that the classification of AGN is dependant on the angle from which they are observed. Features such as jets are not present in all sources. Seyfert type 1 galaxies can be seen identified in the top right corner with a direct view of the central engine (Zackrisson, 2005).

Narrow-Line for objects defined by their broad lines may seem contradictory, but it is actually referring to some of these broad lines being more narrow than expected. More specifically, the hydrogen emission lines from the Balmer series present in the broad-line region are more narrow than in other Seyfert 1 galaxies (Komossa, 2007).

Narrow-Line Seyfert 1 galaxies are useful to study because of the information obtained from the accretion disk region. In particular, when NLS1 galaxies contain the aforementioned radio jets, their spectral data could contain information regarding the interaction between the in-flowing accretion region and the out-flowing jet region, which, on the surface, appear to be two opposing processes. (See Section 1.5).

1.2 BAYESIAN STATISTICS

Bayesian statistics is a method of determining statistical probabilities of events that allows for one to take into account any prior knowledge or biases that one determines might be impactful. Bayesian statistics acts as an alternative approach to the classical frequentist statistics (Halls-Moore, 2022).

While frequentist statistics expresses probabilities as a function of previous outcomes, Bayesian statistics allows for prior assumptions to be made, and then adjusted and updated to a posterior conclusion in light of new evidence.

Bayesian statistics hinges on the theorem known as **Bayes' Rule**. Bayes' Rule relates the probability of an outcome as a function of a condition to the probability of that condition as a function of the outcome. It is derived using the definition of conditional probability:

$$P(A|B) = \frac{P(A \cap B)}{P(B)} \tag{1.1}$$

Equation 1.1 states that the probability of A occurring once B has occurred is equal to the probability of them both occurring together divided by the probability of B occurring. Combining this equation with the inverse equation, that is, the equation for P(B|A), using algebra, Bayes' Rule is derived:

$$P(A|B) = \frac{P(B|A)P(A)}{P(B)} \tag{1.2}$$

One can view A and B as a prior belief and new evidence that is produced,

respectively. With this interpretation, P(A|B) actually represents that probability that the prior belief (called the *prior*) is true, given the new data that has come to light. P(B|A) represents the probability that new evidence will be produced if the prior is true. Therefore, equation 1.2 is ultimately representing the probability of a prior being true given the data. This final probability is called the *posterior*.

1.3   CASH STATISTIC

Cash Statistic, or *C-Statistic* (not to be confused with the *concordance statistic* often used in clinical studies), is a statistical method for determining the quality of a fit, called the "goodness of fit", between a model and data, as well as determining parameter values for a model fit to data. It is a method very similar to the more familiar χ^2 (or Chi-Squared) statistical method (Schmahl, 2005). The C-Statistic method is one that is particularly useful in X-ray astronomy due to the prevalence of low count rates, as it is successful at determining parameter estimations at low count rates (Cash, 1979). The C-Statistic begins by defining the probability of obtaining a result as:

$$P = \prod_{i=1}^{N} \frac{e_i^{n_i} e^{-e_i}}{n_i!} \tag{1.3}$$

where N is the number of bins, e_i is the number of counts per bin, and e_i is the end result of counts in each bin. The C-Statistic is then calculated as a function of this probability P:

$$C = -2\ln P = -2\sum_{i=1}^{N}(n_i \ln e_i - e_i - \ln n_i!) \qquad (1.4)$$

This is done in order to compute a confidence interval around a maximum like-lihood value of P. In order to finally compute a C-Statistic that is a function of the expected counts $E = \sum e_i$, the final equation becomes:

$$C = 2(E - \sum_{i=1}^{N} n_i \ln e_i) \qquad (1.5)$$

This equation can be used to calculate confidence intervals for model parameters when fitting a model to sources, even in the case when there are very few counts per bin. Equation 1.5 is the final equation for determining the ideal parameter values. This is used by XSPEC (see Section 1.4.1) to determine fit quality.

1.4 BAYESIAN X-RAY ANALYSIS

Bayesian X-ray Analysis, or *BXA* (Buchner et al., 2014), is a spectral analysis software package that can be used in tandem with the spectral modelling software **XSPEC** (Arnaud, 1996). It is designed to combine XSPEC with **Ultranest** (Buchner, 2019), the nested sampling algorithm that uses Bayesian statistics to compare user-defined mathematical models.

Since Bayesian statistics benefits from the use of priors and does not rely fully on repeated trials like frequentist statistics (Halls-Moore, 2022), it can be beneficial to use a Bayesian approach when dealing with limited data. In the example of spectral

analysis, frequentist statistics can be valuable when dealing with spectra containing a high number of source counts. However, when dealing with data with low count rates, Bayesian statistics is beneficial because it can make use of the prior understandings of the models.

1.4.1 XSPEC

XSPEC is a spectral modelling tool developed by Keith Arnaud, Craig Gordon, and Ben Dorman with *HEASARC Software Development* in NASA's Astrophysics Science Division. XSPEC is designed to load in high energy spectra and fit them with mathematical models. There are many options for models and the statistics used to determine the quality of the fit between the data and the models.

In addition to its spectral modelling capabilities, XSPEC is also able to generate simulated spectra based off input models. This simulation process effectively makes a spectrum in the shape of an input model and adds noise to the spectrum to simulate real data and uncertainties.

PyXspec is a programming package in the *Python* language designed to interface with XSPEC, which is typically used with the language *TCL*. PyXspec is often used for scripting processes in XSPEC, rather than creating scripts in BASH that use TCL. BXA itself is a Python package, and therefore can only be used with PyXspec.

1.4.2 ULTRANEST

UltraNest is a Python programming package that uses Bayesian statistics to find optimal model parameters. This is done using a technique known as **Nested Sampling**. Nested Sampling explores all possible values for parameters in a parameter space using a user-defined prior distribution, and producing a posterior distribution of parameter values that optimize a given model. This technique also produces a value to assess the likelihood that the model is optimized, called Z. This Z value acts as the evidence for improved fits, and can be used to compare and contrast models once their posterior distributions have been calculated. UltraNest produces its posterior distributions using the logZ value.

Bayesian evidence is considered decisive if it is above 100. That means that a change in logZ of 2 would produce a decisively better model (Buchner, J. et al., 2014). Furthermore, a change in logZ of 1 (Z = 10) would be considered "strong evidence", though not definitive. These logZ values are used to determine the optimal model.

1.5 THESIS OVERVIEW

The goal of this thesis is to analyse spectra of multiple Narrow-Line Seyfert 1 galaxies that have been observed in X-ray bands and also have corresponding radio data (Berton et al., 2018) using Bayesian X-ray Analysis and C-Statistics. More specifically, the objective is to determine if Bayesian X-ray Analysis can provide unique insight into these sources by producing results that the standard C-Statistic approach to spectral modelling could not produce. By analyzing these source spectra, as well

as simulated spectra, in both C-Statistic and BXA, the two statistical approaches can be compared on their ability to consistently measure certain spectral features.

The sample being analysed includes 9 radio loud objects and 12 radio quiet objects. Many of these objects also have multiple observations, resulting in several spectra to analyse. Using XSPEC, these X-ray spectra have been fit with mathematical models that focus on the prominence of the Fe-Kα line in the spectra. This same model is applied to the simulated spectra. Comparing the data between BXA and C-Statistic will demonstrate which approach is more effective at detecting Fe-Kα lines in X-ray spectra.

This thesis will first describe the way spectra are simulated and then modelled using both a C-Statistic and a Bayesian approach (See Chapter 2). Following that, the previously used modelling techniques will be applied to the sample of real sources, and the results from these models will be presented and discussed (See Chapter 3). Lastly, the results will be summarized, final conclusions will be drawn, and areas of future work will be discussed (See Chapter 4).

Chapter 2

SIMULATIONS

In order to compare the effectiveness of C-Statistic and BXA at detecting certain spectral features, specific features to search for must be chosen, and a mathematical model to detect these features must be created. The procedure of this thesis involves choosing a model to fit a specific energy band of the spectra (Section 2.1), then creating thousands of simulated spectra to fit en masse (Section 2.2). The quality of these fits will be analyzed separately, using both C-Statistic (Section 2.3) and BXA (Section 2.4). Following this, the same models will be applied to real data, and the quality of their fits will be analyzed and discussed.

2.1 MODELLING SPECTRA

As previously stated, one of the most prominent features in AGN spectra is the Fe-Kα line(s) around 6.4 keV. Additionally, it was noted that the continuum from approximately 2-10 keV takes the shape of a simple power law. This combination of a simple continuum and a prominent feature makes this 2-10 keV band of an X-ray spectrum an ideal band to investigate the efficacy of two statistical approaches to spectral modelling.

Therefore, the model chosen for this thesis is one that contains two main components: a power law and a Gaussian profile. The former serves the purpose of

modelling the continuum, and the latter fits the shape of an emission line breaching the continuum. In XSPEC, these two components are listed as `powerlaw` and `gauss`, respectively.

When modelling the simulated spectra, this is the complete model that is used. When applying the model to real data, XSPEC provides model components for both the power law and Gaussian profile that take into account the redshift of the source being modelled. This allows the distance of the source to be accounted for when it is modelled. These components are called `zpowerlw` and `zgauss`, respectively. The individual parameters for the components of this model can be seen and described in Table 2.1.

2.2 SIMULATING SPECTRA

As mentioned in Section 1.4.1, XSPEC has the capability to simulate spectral data in the shape of a chosen input model. For instance, when given the aforementioned

Table 2.1: XSPEC Model Parameters

Component Name	Parameter Name	Definition
`powerlaw, zpowerlw`	PhotonIndex (γ)	Determines the slope of the power law.
`powerlaw, zpowerlw`	Norm	Determines the normalization of the power law.
`gauss, zgauss`	LineE	Determines the energy on which the Gaussian will be centered.
`gauss, zgauss`	Width (σ)	Determines the width of the Gaussian profile.
`gauss, zgauss`	Norm	Determines the normalization of the Gaussian profile.
`zpowerlw, zgauss`	z	Determines the redshift by which to calibrate the component.

`powerlaw + gauss` model with certain parameters, XSPEC can simulate a spectrum that takes the shape of that model and adds noise to it to resemble real data counts. The parameters of the model, such as the normalization, can determine the source counts in the simulated spectrum, as well as the strength of spectral features measured by their *equivalent width*, or *EQW*.

Since the process of simulating spectra incorporates randomized noise, it is useful to mass-produce these simulated spectra to determine how reliably certain features are discernible from the noise. Observations can vary in terms of the quality of data obtained due to different objects being observed for different durations. Therefore, it is important to simulate spectra with a wide range of source counts. Additionally, certain AGN have more prominent emission lines than others, so it is also important to simulate spectra with a wide range of EQW values for the Fe-Kα line.

In order to produce the most meaningful results, 1000 spectra were simulated with a specific number of source counts and a specific EQW for the Fe-Kα line. This process was then repeated with a different set of counts and EQW values with the goal of populating a grid (See Figure 2.1a) in a plot of *Counts vs EQW* in order to map out regions of reliable detectability (See Figure 2.1b) based on C-Statistic and BXA.

Once a grid of simulated spectra has been created, each of these spectra can be fit with the input model to detect the Fe-Kα line, using both a C-Statistic and a BXA approach, and the detection rate at each point along the grid will be used to generate confidence lines on the plot.
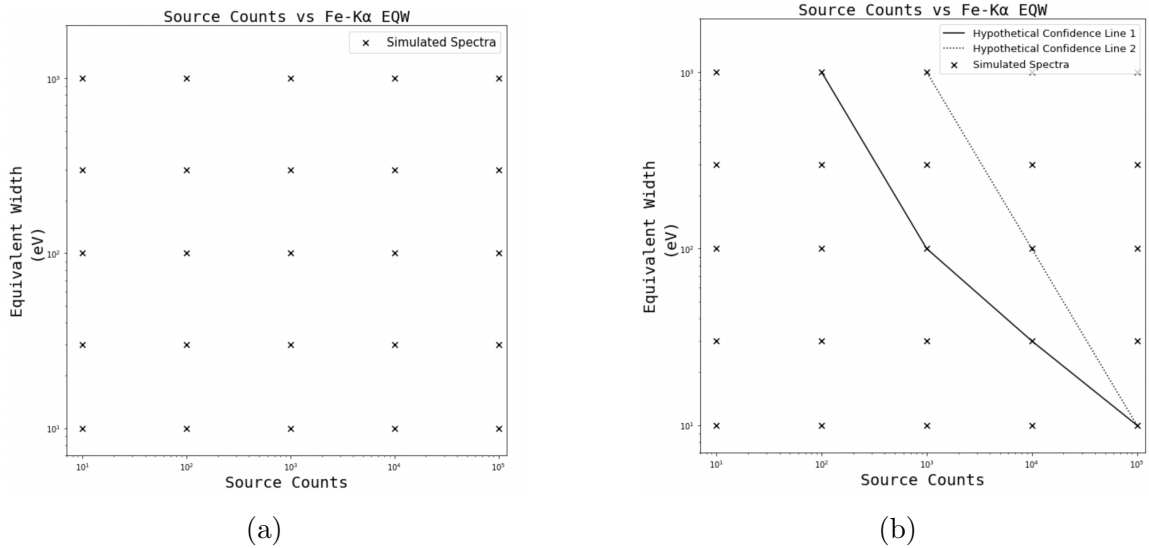
Figure 2.1: Figure 2.1a shows a blank *EQW vs Counts* plot to demonstrate how the simulated spectra will be used to determine regions of reliable detectability. Each data point represents 1000 simulated spectra. Figure 2.1b shows hypothetical confidence lines that could be interpreted from detection rates of the simulated spectra.

2.3 C-STATISTIC APPROACH

Fitting a spectrum with a simple model using the C-Statistic approach is a relatively quick process. In XSPEC, the spectrum is loaded in, and C-Statistic can be selected as the fitting statistic using the `statistic cstat` command. A model can immediately be defined to apply to the spectrum using the `model powerlaw + gauss` command.

The model parameters (See Table 2.1) must be input as starting points to begin assessing the fit with. For the `power law` parameters, γ is estimated as a slope of 2, and norm is estimated as 1. Regarding the `gauss` component, the LineE parameter is estimated as 6.4 keV. The sigma value is selected to be 1 eV, and it is frozen at that value. This ensures that the model is searching for narrow lines in all sources, while the other parameters are allowed to vary. The normalization of the line is chosen based on the EQW of the line in the simulated model (See Table 2.2). Once all the

parameters are selected, the model is applied to the data using the `fit` command,
and a plot of the spectrum and model is output (see Figure 2.2).
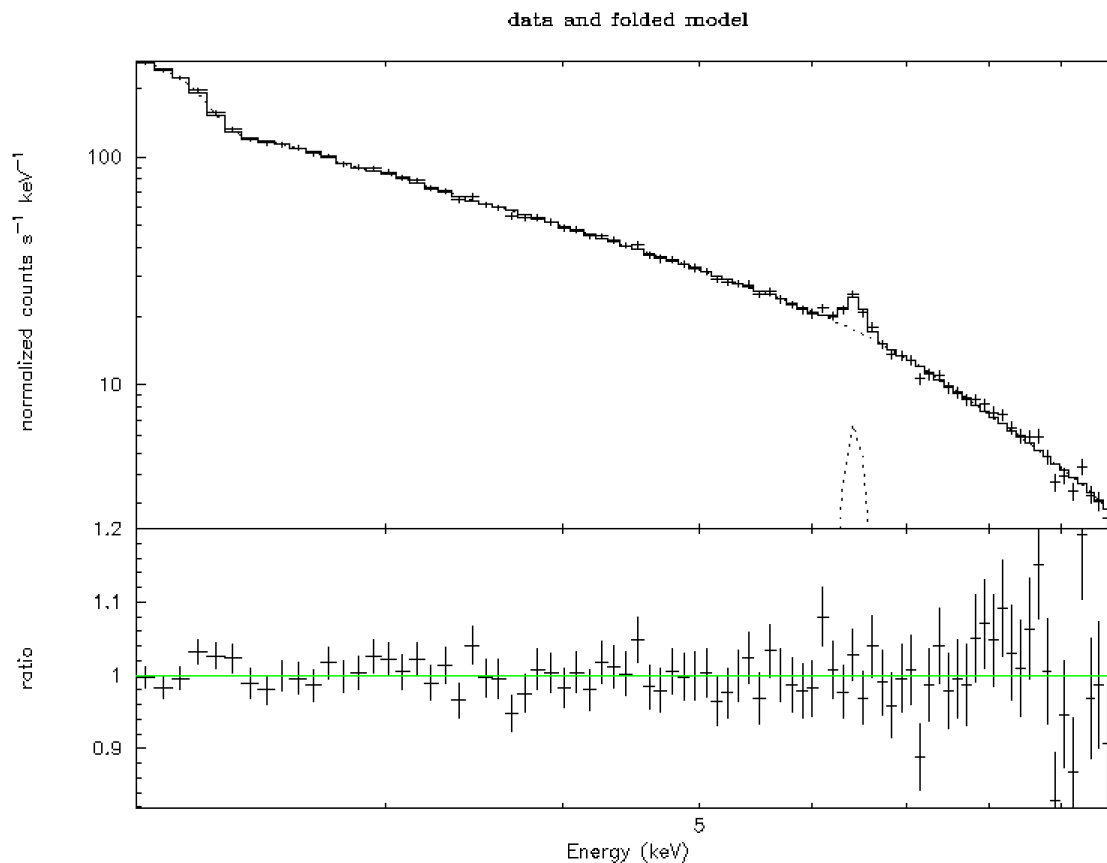
Figure 2.2: Simulated spectrum of an AGN fit with a `powerlaw + gauss` model. The
bottom panel displays the ratio of the spectrum to the model.

XSPEC outputs the resulting fit statistics, including the optimal parameter values.
The final parameter values are recorded, as well as the C-Statistic value and the
number of PHA bins. The above process is then repeated on the same spectrum
with the `gauss` component removed. The fit is again assessed on just the `powerlaw`,
and the output values are recorded. In order to assess if the fit was a significant
improvement when the Gaussian was included, the change in the C-Statistic value is
calculated.

Fit improvement of 2 parameters at 90% significance level
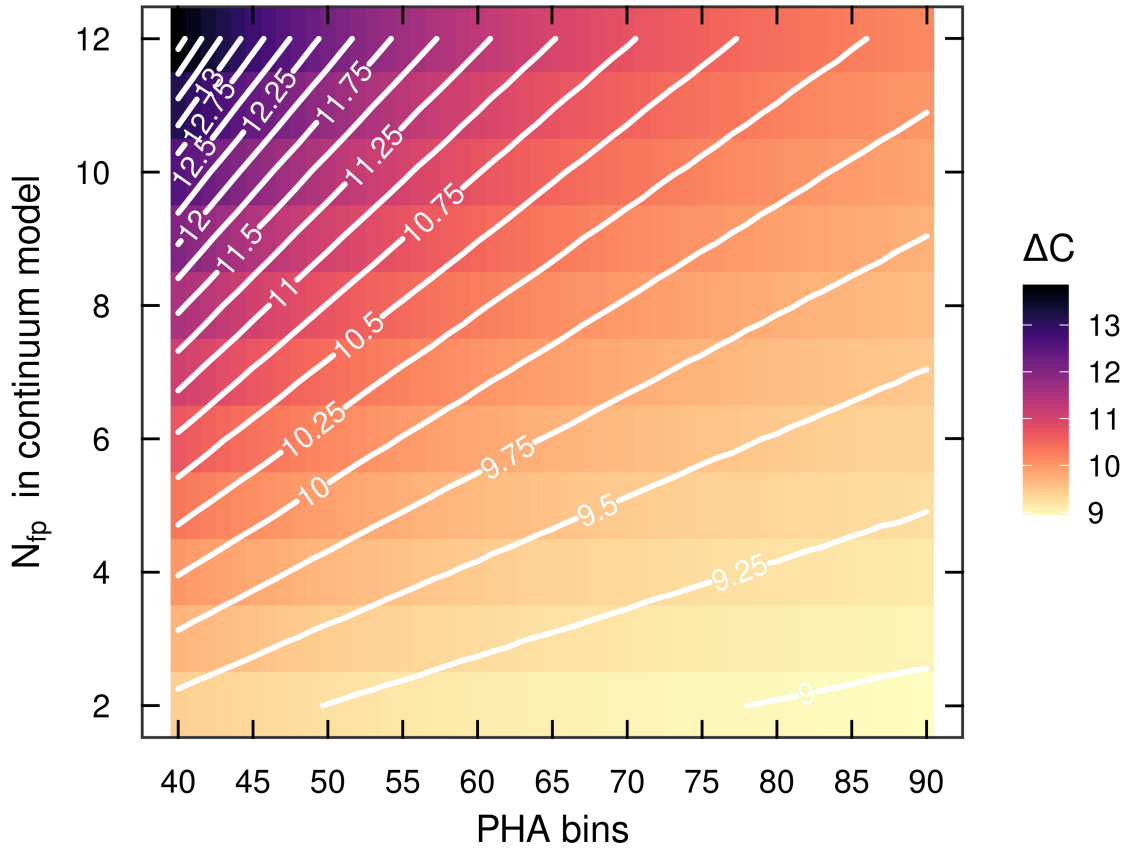
Figure 2.3: This plot shows the ΔC value that would produce a fit improvement with the inclusion of the Gaussian to model the Fe-Kα line at a 90% significance level. It is shown as a function of the number of free parameters in the continuum model (N_{fp}) and the number of binned counts in the spectrum (PHA bins). Figure provided by Dr. Adam Gonzalez.

This change in the C-Statistic value is called the ΔC. In order to determine when a fit is sufficiently improved, a threshold for ΔC must first be determined. This was done using a correction to Akaike's Information Criterion (AIC) to account for small sample sizes (called AICc) (Sugiura, 1978). Figure 2.3, provided by Dr. Adam Gonzalez, shows the ΔC values that meet the necessary threshold as a function of the model parameters and number of data points, as per the AICc function.

The entire above process is then scripted to be done en masse to all 1000 spectra

Table 2.2: Gaussian Normalization from Fe-Kα EQW

Fe-Kα EQW (eV)	Normalization
10	0.00025
20	0.0005
30	0.00075
40	0.001
60	0.0015
100	0.0025
200	0.005
300	0.0075
400	0.01
500	0.0125
700	0.0175
1000	0.025

at a given combination of EQW and source counts. This process is then done at each combination of EQW and source counts, and for each set of 1000 spectra, the percentage of spectra with a sufficient ΔC is calculated. A line can then be drawn connecting points on the resulting grid to determine at which values of EQW and source counts a line can be reliably detected.

2.4   BXA APPROACH

Running BXA on a spectrum, or a set of spectra, is a lengthier process. For each spectrum, the UltraNest algorithm steps through the full parameter space to find the ideal fit and also produce posterior distributions for each parameter. Similarly to the C-Statistic approach, the BXA approach involves analyzing the fit between the model and the data using one model with the Gaussian component, and one without it.

Firstly, a python script is run that loads in a simulated spectrum as the input spectrum, and then fits this spectrum with a `powerlaw + gauss` model. Priors are

then selected for each of the parameters that are being varied: γ, LineE, and the normalization of both components. As was the case with the C-Statistic approach, the width (σ) parameter is kept frozen. The γ and LineE parameter spaces are explored using uniform priors, with the slope ranging from 1-4, and the LineE value ranging from 5-10 keV. The normalization parameter spaces are both explored using Jeffery's priors, which creates a uniform distribution in logarithmic space, each bound between 10^{-3} and 1. The BXA package is then run on the spectrum, outputting posterior distributions of all the parameters (see Figure 2.4), as well as logZ values.

This process is then repeated without the `gauss` component, and the logZ values are compared. As mentioned in Section 1.4.2, a ΔlogZ value of 1 or more is considered strong evidence for fit improvement, and is therefore the threshold used in this thesis.

All the simulated spectra are fit with this process and then the ΔlogZ values are compared. The percentage of simulated spectra that have sufficient ΔlogZ are recorded. Ultimately, the results from the simulated spectra allow a grid of detectability to be produced from BXA, and the results from the real data allow the real spectra to be compared between the two statistical methods (see Section 3.3).

2.5 SIMULATION RESULTS

The first result is obtained by running a C-Statistic fit on all of the simulated spectra and recording the rate of detection of the Fe-Kα line. Then, plotting these detection rates as a function of the source counts in the spectra and the EQW of the Gaussian line, a line can be drawn to connect the points on this plot that were detected
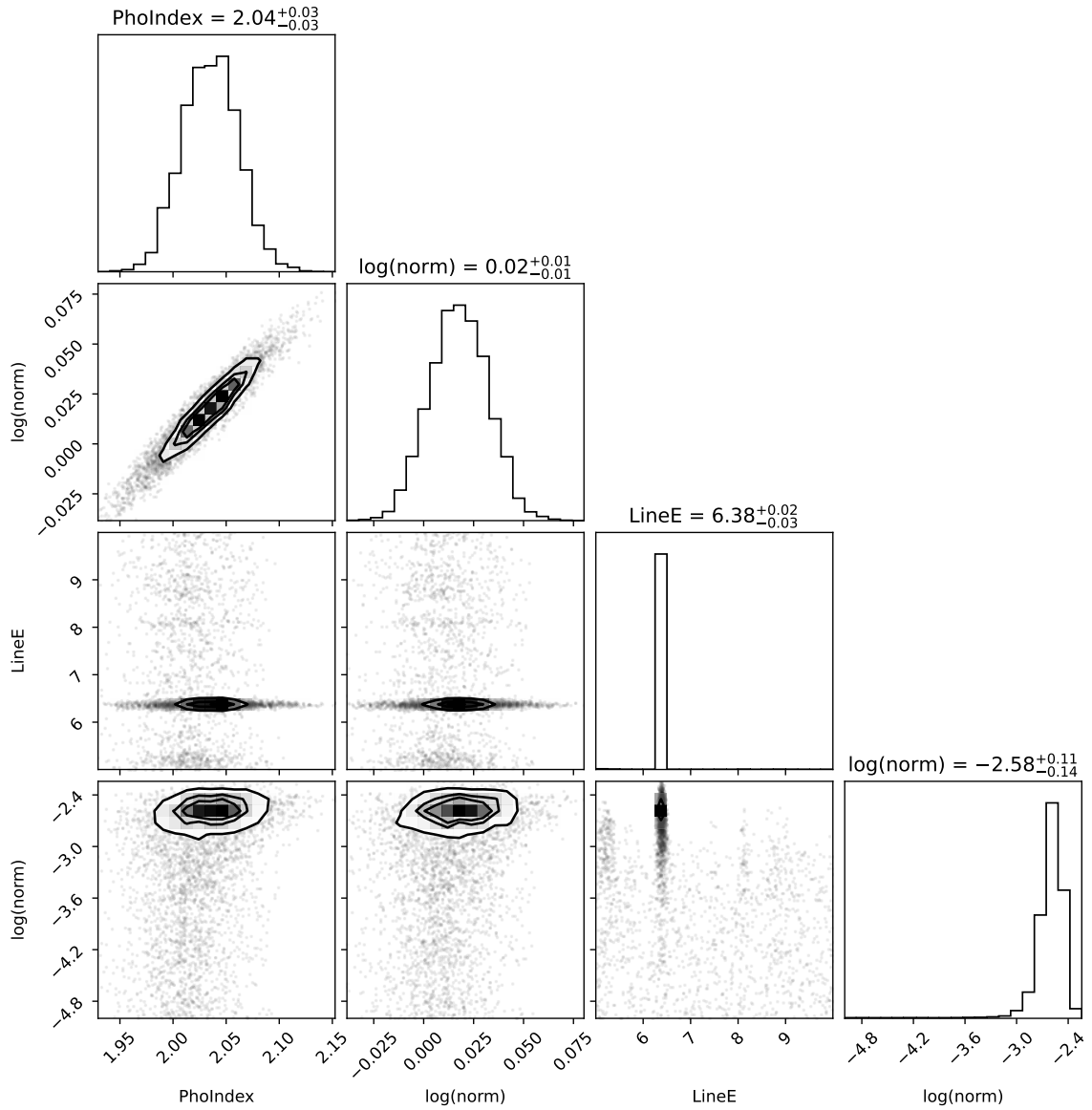
Figure 2.4: Corner plot displaying the posterior distributions of all model parameters, output by BXA.

approximately 50% of the time. Next, the results from running a BXA fit on all of the simulated data are plotted in the same manner (See Figure 2.5). These two confidence lines can be contrasted and the general trends of their detection capabilities as a function of source counts and emission feature EQW can be compared.

This result directly contrasts how reliable C-Statistic and BXA are at detecting
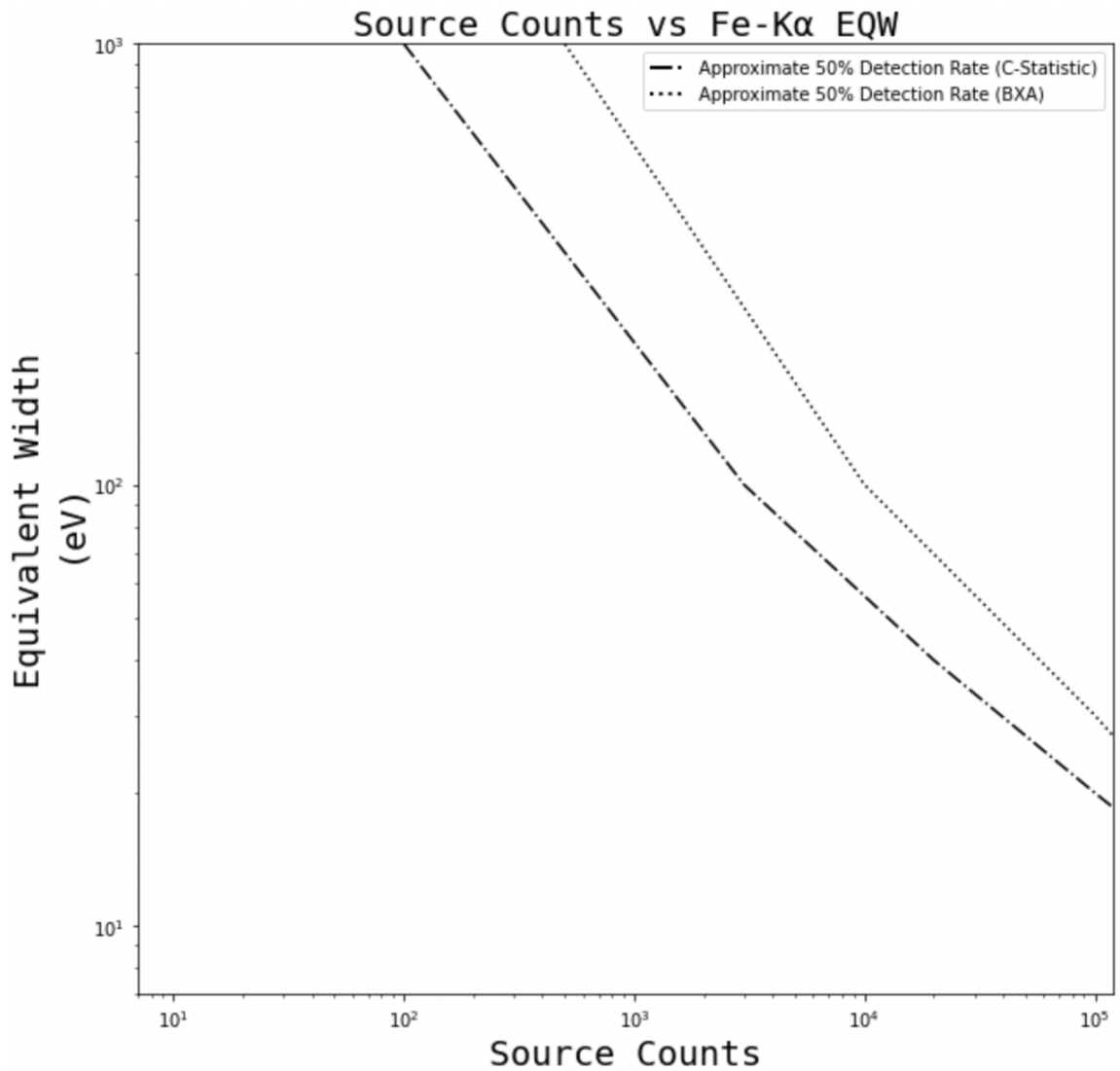
Figure 2.5: Plot of Fe-Kα EQW against source counts with the 50% detection rate lines from both BXA and C-Statistic compared.

the presence of an Fe-Kα emission line in a spectrum, given a certain prominence of the feature and a number of source counts. From Figure 2.5, it seems that at any given equivalent width or number of source counts that C-Statistic can detect emission features more reliably. The C-Statistic method produces higher detection rates at lower source counts and at lower equivalent widths. Alternatively, this result could also imply that the 90% significance criterion used in the C-Statistic approach

is a less strict criterion than that of the BXA approach.

Proceeding with modelling real sources, this data will help explain any null detections in certain sources with low count rates. From this result, it is expected that sources with count rates far below both 50% confidence lines will not produce an Fe-Kα emission line, and that this is not evidence for the absence of an emission line in that spectrum. Furthermore, it is expected that the C-Statistic method will detect Fe-Kα emission lines in more of the sources with lower counts than the BXA approach.

Chapter 3

TESTING AGN DATA

After testing both the C-Statistic and BXA approach on several thousand simulated spectra, these models must now be applied to real data. Using a sample of 21 objects (Section 3.1), the previously described methods will be used to search for Fe-Kα emission lines in the spectra of these objects using both C-Statistic and BXA (Section 3.2). The results from fitting these models will then be presented and discussed (Section 3.3).

3.1 SAMPLE

As mentioned in Section 1.5, the sample of real data is a set of Narrow-Line Seyfert 1 galaxies that were previously analyzed in the radio band (Berton et al., 2018). The X-ray spectra of all the sources have been obtained by the XMM-Newton Telescope. By separating the sources into radio loud and radio quiet designations, any further trends seen between these two types of objects could be attributed to radio-related processes, which would be an interesting secondary conclusion drawn from the sample. Table 3.1 contains a list of all the used sources and their observations IDs, as well as their designation in terms of their radio loudness, simply as radio loud or radio quiet.

Table 3.1: Source Observations and Information

Source Name	Observation ID	Radio Loud/Quiet
FBQSJ07580039202	0406740101	Loud
IRAS 17020+4544	0206860101	Loud
IRAS 17020+4544	0206860201	Loud
IRAS 17020+4544	0721220101	Loud
IRAS 17020+4544	0721220301	Loud
IRAS 16319+4725	0673270101	Loud
IRAS 16319+4725	0673270201	Loud
IRAS 16319+4725	0673270301	Loud
IRAS 16319+4725	0673270401	Loud
IRAS 06269-0543	0153100601	Loud
SDSS J124634.65+023809.0	0690090201	Loud
PKS 1502+036	0690090101	Loud
FBQS J1102+2239	0690090301	Loud
FBQS J154817.9+351128	0674320301	Loud
FBQS J154817.9+351128	0674320401	Loud
RE J1034+396	0561580201	Loud
RE J1034+396	0655310101	Loud
RE J1034+396	0655310201	Loud
RE J1034+396	0675440101	Loud
RE J1034+396	0675440201	Loud
RE J1034+396	0675440301	Loud
RE J1034+396	0824030101	Loud
ARK 564	0006810101	Quiet
ARK 564	0006810301	Quiet
ARK 564	0206400101	Quiet
ARK 564	0670130201	Quiet
ARK 564	0670130301	Quiet
ARK 564	0670130401	Quiet
Mrk766	0096020101	Quiet
Mrk766	0109141301	Quiet
Mrk766	0304030101	Quiet
Mrk766	0304030301	Quiet
Mrk766	0304030401	Quiet
Mrk766	0304030501	Quiet
FBQSJ16294007	0784521301	Quiet
UGC3478	0654800401	Quiet
Mrk493	0852060201	Quiet
WAS61	0843020601	Quiet
SBS1118541	0741031301	Quiet
Mrk705	0783270401	Quiet
Mrk110	0201130501	Quiet
Mrk335	0306870101	Quiet
PG1244026	0675320101	Quiet
IRAS133492438	0852390101	Quiet

3.2 MODELLING REAL DATA

The process of modelling real data using XSPEC, both in the C-Statistic and BXA approach, is fundamentally the same as explained in Sections 2.3 and 2.4. The key difference is that real data are found at a variety of distances and, consequently, a variety of redshifts. XSPEC contains variations of the model components with an added parameter to account for the redshift of a source (shown in Table 2.1).

When modelling the real sources, these altered model components must be used. Therefore, rather than using a `powerlaw + gauss` model, a `zpowerlw + zgauss` model is used, where the z represents the redshift parameter. This in an input parameter that is not given the freedom to vary, and it depends on each individual source's redshift.

After adjusting for the redshift in each source, the procedure is the same as previously explained: The sources are fit using both the C-Statistic and BXA approach, and the significance of any detected Fe-Kα line is determined by each approach's significance threshold.

3.3 AGN RESULTS

In the first result obtained by fitting the real AGN data, the results from running a C-Statistic fit on all of the real observations are plotted as a function of each source's number of source counts and the EQW of the emission feature. The confidence line obtained in the previous chapter by using C-Statistic on the sources is overlaid with the data (see Figure 3.1). Using the same criteria for detection as mentioned in

Section 2.3, the real data display whether or not they contain an Fe-Kα line that was detected by C-Statistic. Hollow points on the figure designate objects where a Gaussian line was fit in the model, but it was not found to be significant.

Next, the same results are plotted with the BXA 50% confidence line overlaid (see Figure 3.2). This result offers an alternative comparison between the detection rate of the sources and that of the simulated data.

Figure 3.1: Plot of Fe-Kα EQW against source counts with the 50% detection rate determined from the simulated spectra using C-Statistic. Detection data from real sources overlaid.

Lastly, the key model parameter from both the BXA and C-Statistic approach can be compared directly (See Figure 3.3). The central energy of the `zgauss` model component was recorded for each observation and they can both be plotted simultaneously. Note that any observations that were found to not detect an Fe-Kα emission line in both BXA and C-Statistic are removed to make the plot easier to read, as the
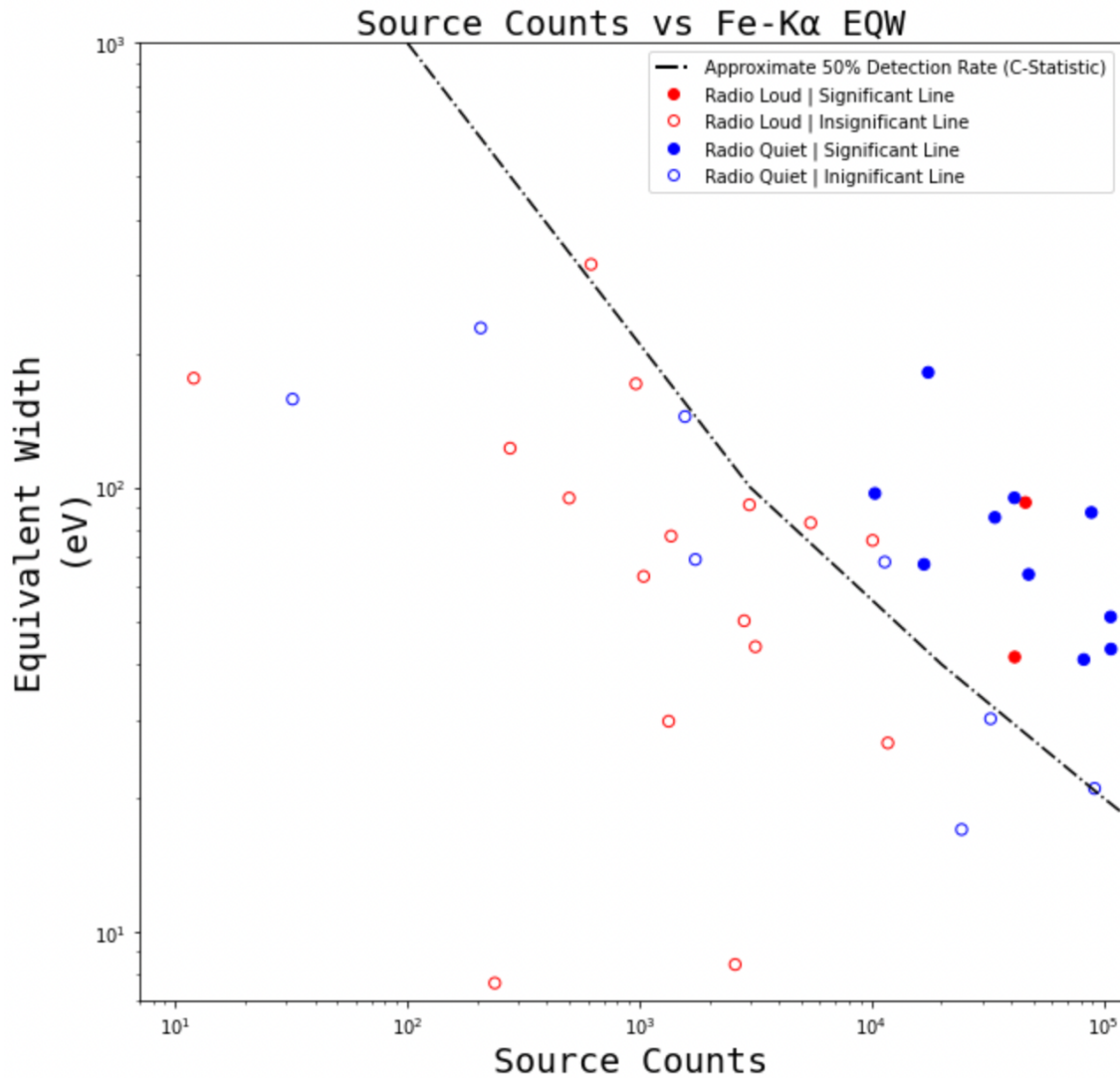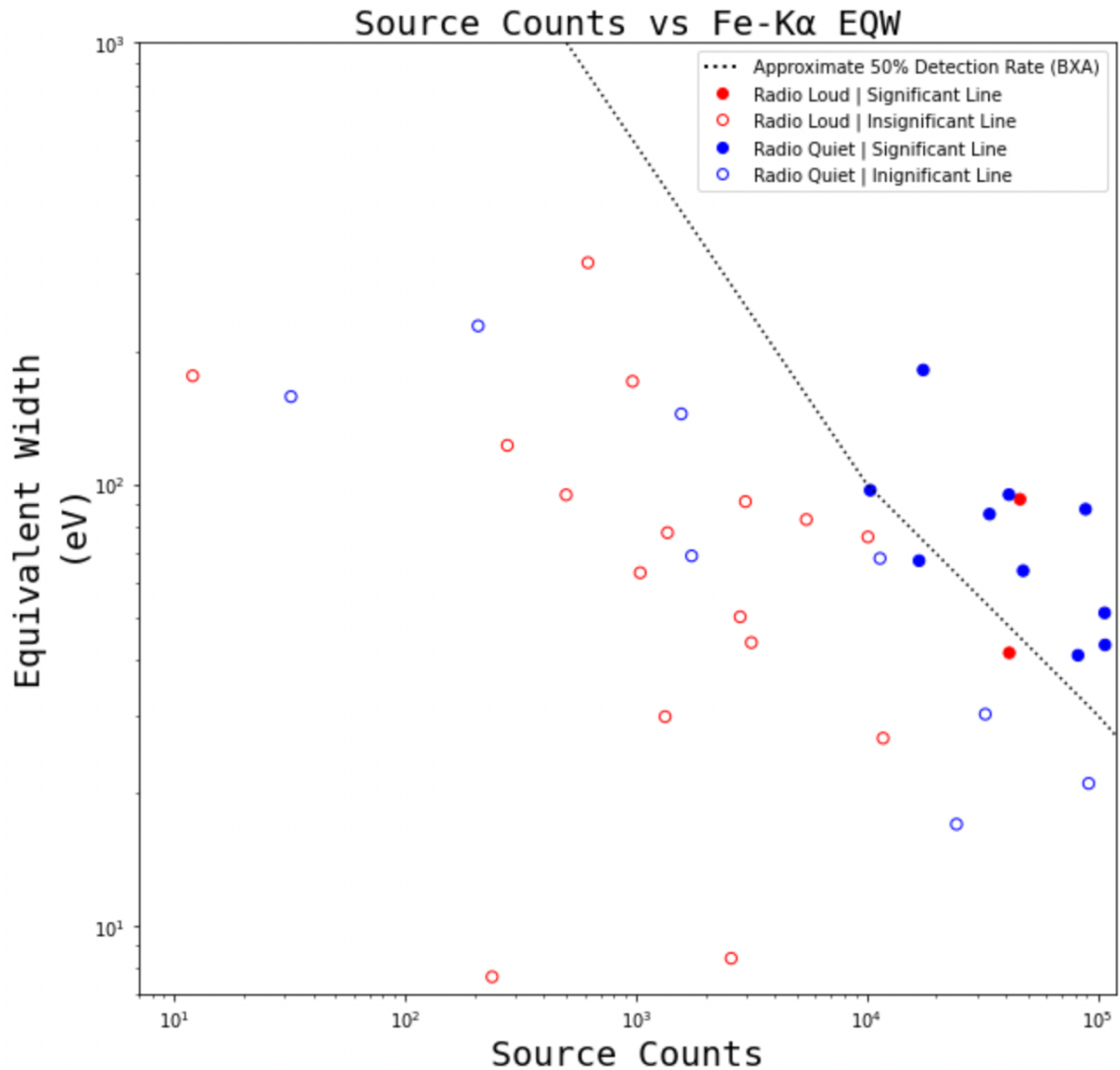

Figure 3.2: Plot of Fe-Kα EQW against source counts with the 50% detection rate determined from the simulated spectra using BXA. Detection data from real sources overlaid.
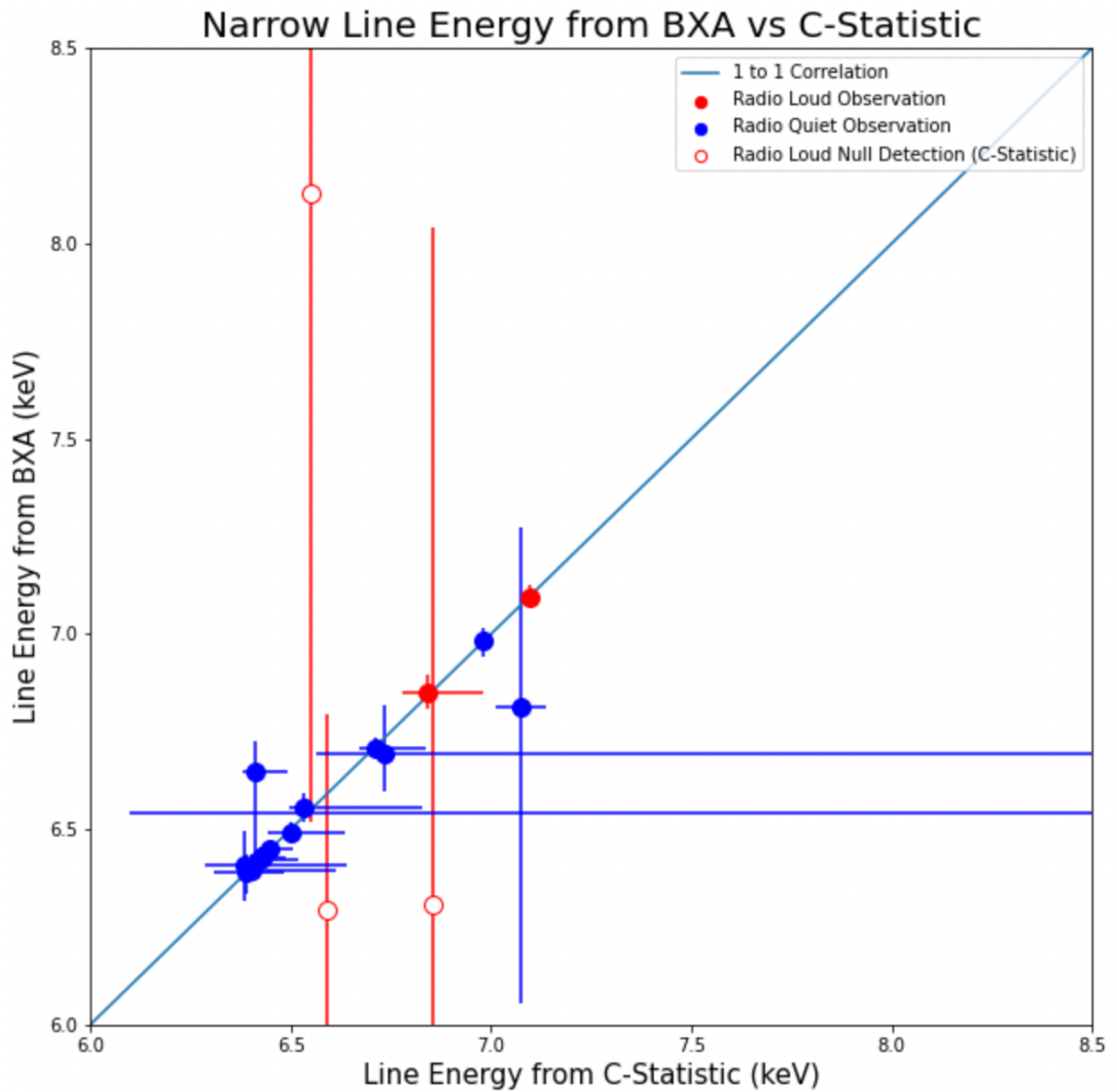
Figure 3.3: Plot of the LineE parameter for the Fe-Kα line in both C-Statistic and BXA, with a line showing the 1 to 1 trend. This is not a line of best fit.

error bars on these insignificant detections are much larger than the others. A line

showing a 1 to 1 trend is also displayed in order to show how correlated the emission

lines are between the two methods of detection.

Chapter 4

DISCUSSION

The result produced by the C-Statistic trials on the simulated data demonstrates that, at a certain number of source counts, an Fe-Kα emission line of a certain strength may not be reliably detectable. On Figure 3.1 it can be assumed that any objects falling along that 50% confidence line can not have a Fe-Kα line reliably detected, if one is present. The general trend of increased detectability increases towards the upper right portion of the plot, which is an area that is more populated by sources that have had Fe-Kα lines detected. In the upper right portion of the plot, relative to the confidence line, there are only four observations that did not have lines detected to a 90% significance. Two of these observations lie in very close proximity to the 50% confidence line, so it can safely be assumed that these observations have a 50/50 chance having their Fe-Kα line detected by this C-Statistic approach, if it is present.

It is also worth noting that the only noticeable difference between the radio loud and radio quiet sources in this plot seems to be that the sample of radio quiet sources is made up of better data. That is to say that the radio quiet sources appear to have higher source counts on average, which is likely due to them being observed for longer durations.

When analyzing Figure 3.2, it can be seen that the approximate 50% confidence line produced by running the BXA fit on all the simulated spectra results in a smaller

area of reliable detectability. It is also worth noting that this line cuts between data points that had lines found to be significant.

This could potentially point to the idea that some of the lines that were detected in some of the sources were false positives, although this is likely not the case, due to a result from Figure 3.3: None of the observations that had lines detected by the C-Statistic approach failed to have lines detected by BXA. This means that all the objects that appear to be detected in Figure 3.2 were detected in BXA and C-Statistic. Since these observations were reliably further to the upper right portion of the plot than the confidence line in the previous figure (Figure 3.1), it is unlikely these are false positives in BXA, though it is still a possibility.

Nonetheless, the difference in the reliability of detecting various emission features between BXA and C-Statistic can be seen more clearly in Figure 2.5, and there is a notable difference. This plot on its own would appear to demonstrate that C-Statistic is more effective at detecting spectral features for low-count observations, and even for weaker features.

The two lines appear to be similar in shape, with neither one showing a preference for lower counts or lower EQW. This is also an interesting result, because it shows that, ultimately, neither source counts nor feature strength appear to be more important than the other in terms of detectability.

As previously noted, Figure 2.5 would appear to demonstrate C-Statistics' superiority when measuring emission lines for low-count sources. However, Figure 3.3 demonstrates the opposite. This result shows, firstly, that all sources that contained lines detected by C-Statistic also had their lines detected by BXA. Furthermore, there

were 3 observations that had lines detected from the BXA approach that were not detected in the C-Statistic approach. When the LineE parameter of all the observations are analyzed, it appears that these 3 observations, that were only detected using BXA, deviate from the general linear correlation the rest of the observations tend to follow. The vast majority of the observations that had lines detected follow a nearly 1 to 1 line.

There is one observation in particular that stands out the most from the trend. The one null detection with a BXA LineE value around 8 is attributed to the source REJ1034+396, observation 0824030101 (See Table 3.1). Considering that this one observation is only one of 7 available for this object, there is no clear reasoning as to why this one particular observation was best fit with a very different Gaussian line than the other objects, or even the other observations of the same object.

Furthermore, it is worth noting the size of the error bars obtained by the BXA approach on the objects that were not significantly detected using C-Statistic. While these observations were found to contain significant Fe-Kα emission lines, there is notably less certainty in their measurement than those that were detected using both methods.

The general results from both the simulated data and the real data also lead to the questioning of any differences in the conditions for fit improvement. For C-Statistic, the chosen threshold was a ΔC that would correlate to a 90% significant improvement of the overall fit. Using a Bayesian approach, the chosen threshold was that the change in Bayesian evidence had to be sufficient to produce "strong evidence" of a fit improvement. If these two thresholds are notably different, it could be the

reasoning behind the difference in detection rate in both the simulations and the real data. This can be further exemplified in the size of the error bars, as previously mentioned. The size of the error bars on the 3 sources that favoured BXA implies that these sources may have nearly not reached the Bayesian significance threshold, and they evidently did not meet the significance threshold for C-Statistic either. The ways in which these 3 sources are outliers of the rest of the sample also indicate that they may be false-positive detections, not by chance, but by measuring a different feature in the spectrum that is unrelated to the Fe-Kα line.

The contradicting results between the simulated data and the real data, however, suggest also that there may be a hidden variable that resulted in BXA measuring lines more effectively in the real data. It is possible that BXA is less effective at finding low-strength lines in low-count data than C-Statistic, but more effective at detecting features in spectra with an unknown trend.

Chapter 5

CONCLUSION

After using C-Statistic and BXA to fit spectral models to thousands of simulated spectra and 21 real Narrow-Line Seyfert 1 sources, the following conclusions were drawn:

- C-Statistic is more effective at finding low-strength emission features in low-count spectra than BXA.

- This effectiveness was not apparent when testing real data, as BXA found emission features more frequently, although these detections could be false-positives.

- There may be more relevant variables than feature EQW and source counts when searching for emission features.

- BXA's 'strong evidence' criterion may differ from C-Statistics' 90% significance criterion, and one may be less precise than the other.

With further research, this difference in the significance threshold for the two methods can be investigated. Rather than using a binary approach of designating detections as either significant or insignificant, each detection can be plotted as a function of their ΔlogZ and ΔC values. This could produce an interesting result regarding how the significance thresholds of each approach align with one another. Additionally, by running more simulations at different values of source counts and

EQW, the resolution of the grids can be improved, and further confidence lines (such as 90%) can be plotted. If other confidence lines of the two approaches align differently than the 50% lines, this could be another interesting result.

To investigate the presence of hidden variables in the sample, it would be useful to extract further data from the models and look for correlations between the model parameters of the objects and the detection of lines. This thesis investigated the correlation between line-detectability and data quality, but there may be further correlations found in the model parameters themselves. This could be investigated using Principle Component Analysis.

Bibliography

K. A. Arnaud. XSPEC: The First Ten Years. In George H. Jacoby and Jeannette Barnes, editors, *Astronomical Data Analysis Software and Systems V*, volume 101 of *Astronomical Society of the Pacific Conference Series*, page 17, January 1996.

M. Berton, E. Congiu, E. Järvelä, R. Antonucci, P. Kharb, M. L. Lister, A. Tarchi, A. Caccianiga, S. Chen, L. Foschini, A. Lähteenmäki, J. L. Richards, S. Ciroi, V. Cracco, M. Frezzato, G. La Mura, and P. Rafanelli. Radio-emitting narrow-line seyfert 1 galaxies in the JVLA perspective. *Astronomy & Astrophysics*, 614: A87, jun 2018.

J. Buchner, A. Georgakakis, K. Nandra, L. Hsu, C. Rangel, M. Brightman, A. Merloni, M. Salvato, J. Donley, and D. Kocevski. X-ray spectral modelling of the AGN obscuring region in the CDFS: Bayesian model selection and catalogue. , 564:A125, April 2014.

Johannes Buchner. Collaborative Nested Sampling: Big Data versus Complex Physical Models. , 131(1004):108005, October 2019.

Buchner, J., Georgakakis, A., Nandra, K., Hsu, L., Rangel, C., Brightman, M., Merloni, A., Salvato, M., Donley, J., and Kocevski, D. X-ray spectral modelling of the agn obscuring region in the cdfs: Bayesian model selection and catalogue. *A&A*, 564:A125, 2014.

W. Cash. Parameter estimation in astronomy through application of the likelihood ratio. , 228:939–947, March 1979.

L. Gallo. Revealing the innermost regions of active galaxies. *Journal of the Royal Astronomical Society of Canada*, 08 2011.

Michael Halls-Moore. Bayesian statistics: A beginner's guide, Apr 2022.

S. Komossa. Narrow-line seyfert 1 galaxies, 2007.

NASA, ESA, S Baum, C O'Dea, R Perley, and W Cotton. *A Multi-Wavelength View of Radio Galaxy Hercules A*. NASA, Nov 2012.

Barbara Ryden & Bradley M. Peterson. *Foundations of Astrophysics*. Pearson Addison-Wesley, 2009.

Ed Schmahl. The cash statistic and forward fitting, 2005.

John S. Gallagher III & Linda S. Sparke. *Galaxies in the Universe: An Introduction*. Cambridge University Press, 2nd edition, 2007.

Nariaki Sugiura. Further analysis of the data by akaike's information criterion and the finite corrections. *Communications in Statistics - Theory and Methods*, 7(1): 13–26, 1978.

Dan Wilkins. Gigantic x-rays flares offer new insight into the whirling maelstrom just outside supermassive black holes. *Kavli Institute for Particle Astrophysics and Cosmology*, June 2017.

Erik Zackrisson. Quasars and low surface brightness galaxies as probes of dark matter. 05 2005.